# Observation of Structure of Surfaces and Interfaces by Synchrotron X-ray Diffraction: Atomic-Scale Imaging and Time-Resolved Measurements

# Observation of Structure of Surfaces and Interfaces by Synchrotron X-ray Diffraction: Atomic-Scale Imaging and Time-Resolved Measurements

Yusuke Wakabayashi[1a], Tetsuroh Shirasawa[2], Wolfgang Voegeli[3], and Toshio Takahashi[3]

[1]*Division of Materials Physics,*

*Graduate School of Engineering Science,*

*Osaka University, Toyonaka 560-8531, Japan*

[2]*National Metrology Institute of Japan,*

*National Institute of Advanced Industrial Science and Technology,*

*Tsukuba 305-8565, Japan*

[3]*Department of Physics,*

*Tokyo Gakugei University,*

*Koganei 184-8501, Japan*

(Dated: January 11, 2018)

[a] e-mail: wakabayashi@mp.es.osaka-u.ac.jp

# Abstract

The recent developments in synchrotron optics, X-ray detectors, and data analysis algorithms have enhanced the capability of the surface X-ray diffraction technique. This technique has been used to clarify the atomic arrangement around surfaces in a non-contact and nondestructive manner. An overview of surface X-ray diffraction, from the historical development to recent topics, is presented. In the early stage of this technique, surface reconstructions of simple semiconductors or metals were studied. Currently, the surface or interface structures of complicated functional materials are examined with sub-Å resolution. As examples, the surface structure determination of organic semiconductors and of a one-dimensional structure on silicon are presented. A new frontier is time-resolved interfacial structure analysis. A recent observation of the structure and dynamics of the electric double layer of ionic liquids, and an investigation of the structural evolution in the wettability transition on a $TiO_2$ surface that utilizes a newly designed time-resolved surface diffractometer, are presented.

## I. INTRODUCTION

X-ray diffraction has been used for crystal structure determination for over 100 years. The scattering amplitude of X-rays is given by the Fourier transform of the electron density. Therefore, in principle, if we obtain the scattering amplitude in a large volume of the reciprocal space, we can observe the electron density distribution of any specimen, regardless of its periodicity or outer shape.

In practice, the scattering intensity at arbitrary points in the reciprocal space is, apart from the Bragg reflections and the signal caused by the thermal vibration, usually far too weak to be measured. One major exception is the scattering from flat surfaces. In this case, there is a finite Fourier component of the electron density in the direction perpendicular to the surface because of the truncation of the crystal. As a result, each Bragg reflection has a rod-shaped tail along the surface-normal direction; this is known as crystal truncation rod (CTR) scattering[1,2]. Similarly, surface superstructures with a different periodicity in the surface plane also give a rod-shaped intensity distribution but it appears at different in-plane positions from the CTRs. The superstructure rods show only a gradual change in the intensity along the surface-normal direction because of the spatially limited out-of-plane extent of the surface structure. In both cases, the rod-shaped intensity distribution reflects the surface structure. By analyzing these intensity distributions, surface X-ray diffraction (SXD) provides not only the in-plane structure but also the depth profile of the structure with sub-Å resolution. The large penetration depth allows us to apply this method to solid-solid or solid-liquid interfaces as well as surfaces in a nondestructive manner. This feature is particularly useful as methods to study interfacial structures are limited. In this review article, the recent developments of the SXD technique are presented.

## II. PRINCIPLE OF SURFACE DIFFRACTION

In this section, an overview of the principle of SXD and the methods used for SXD measurements is given, following the historical development.

### A. Grazing-incidence diffraction and in-plane diffraction

The challenge of SXD is to measure the weak signal from one or a few atomic layers at the surface among the much larger number of layers in the whole sample. This is possible because the SXD intensity appears at different positions in the reciprocal space compared with the diffracted intensity from the bulk. Nevertheless, in many cases, it is necessary to reduce the diffuse background from the bulk and to reduce the amount of data needed to deduce the two-dimensional structure specific to the surface. Grazing-incidence X-ray diffraction (GIXD) and in-plane diffraction are two approaches that have been used for this purpose.

When the glancing angle of the incident X-rays is less than the critical angle of total reflection, typically 0.2–0.5°, the penetration depth of the X-rays is less than 100 Å, which is three to four orders of magnitude smaller than the penetration depth of X-rays incident normal to the surface. Because of this reduction in penetration depth, the background scattering by the substrate, which is proportional to the illuminated volume, is greatly reduced. Total reflection is a phenomenon involving multiple scattering processes as the evanescent wave is excited in the substrate but the scattering is well approximated by kinematical theory when the glancing angle of the X-rays is more than a few times larger than the critical angle[3,4]. For this reason, the glancing angle of incident X-rays is usually set outside the total reflection region for precise structure measurements, which still provides a considerable reduction in the background. This GIXD geometry is often used in SXD measurements.

In the in-plane geometry, the incident and exit beams both make a glancing angle with the sample surface. The scattering vector is then nearly parallel to the surface, and the diffracted intensity reflects the two-dimensional structure projected onto the surface. The reduction of the dimensionality allows us to obtain the in-plane structure from a comparatively small number of diffraction spots.

### B. Out-of-plane diffraction

To obtain structural information perpendicular to the surface, it is necessary to use the out-of-plane geometry, where the incident or exit beam makes a large angle with the substrate surface. Usually, the incident beam is set to a grazing angle to suppress the background

scattering except in specular rod (i.e., the rod passing through the origin of the reciprocal space) measurements.

Since X-rays penetrate deep into the crystal, a semi-infinite crystal truncated at the surface contributes to the diffraction phenomenon, which is CTR scattering. According to kinematical theory, the CTR scattering amplitude from a perfect crystal with a flat surface parallel to the $a$- and $b$-axes is given by

$$\begin{aligned} F^{\mathrm{B}}(\boldsymbol{Q}) &= F_{hk}(l) \sum_{n=0}^{-\infty} \exp(2\pi \mathrm{i} n l) \\ &= \frac{F_{hk}(l)}{1 - \exp(-2\pi \mathrm{i} l)}. \end{aligned} \tag{1}$$

Here, $F_{hk}(l)$ is the scattering amplitude from one atomic layer of the crystal and $\boldsymbol{Q}$ is the scattering vector defined by $\boldsymbol{Q} = h\boldsymbol{a}^* + k\boldsymbol{b}^* + l\boldsymbol{c}^*$, where $h$ and $k$ are integers denoting the integral-order rod and $l$ indicates a point on the $hk$ rod; $\boldsymbol{a}^*$, $\boldsymbol{b}^*$, and $\boldsymbol{c}^*$ are the reciprocal lattice vectors.

When the surface of the crystal has a structure different from the bulk, the total scattering amplitude is described as

$$F(\boldsymbol{Q}) = F^{\mathrm{B}}(\boldsymbol{Q}) + F^{\mathrm{S}}(\boldsymbol{Q}), \tag{2}$$

using the scattering amplitude from the surface structure $F^{\mathrm{S}}(\boldsymbol{Q})$. Then, the total diffracted intensity $I(\boldsymbol{Q})$ from the crystal with the surface structure is given as

$$\begin{aligned} I(\boldsymbol{Q}) &= C(\boldsymbol{Q}) |F(\boldsymbol{Q})|^2 \\ &= C(\boldsymbol{Q}) |F^{\mathrm{B}}(\boldsymbol{Q}) + F^{\mathrm{S}}(\boldsymbol{Q})|^2, \end{aligned} \tag{3}$$

where $C(\boldsymbol{Q})$ is a combination of proportional factors depending on the experimental conditions, such as the scale factor, polarization factor, and Lorentz factor.

Figure 1 shows the rod profiles for a simple cubic crystal calculated by Eq. (3). The dotted curve is the intensity profile of the CTR scattering from a perfect crystal given by $|F^{\mathrm{B}}|^2$. The solid curve was calculated for a crystal whose top layer was relaxed inward by 5%. It should be noted that the CTR scattering amplitude $F^{\mathrm{B}}(\boldsymbol{Q})$ changes its phase by $\pi$ at the Bragg points[5]. Thus, the interference effect between $F^{\mathrm{B}}(\boldsymbol{Q})$ and $F^{\mathrm{S}}(\boldsymbol{Q})$ brings about the asymmetric profile around the Bragg points, as seen in the solid curve. Moreover, the CTR intensity at an anti-Bragg point, where $l$ is a half-integer, is given by $|F_{hk}|^2/4$ from Eq. (1), that is, less than the diffracted intensity from a single layer. Therefore, SXD is

sensitive to the surface structure $F^{\mathrm{S}}(\boldsymbol{Q})$. CTR scattering has also been used to investigate the roughness at surfaces[2,6].

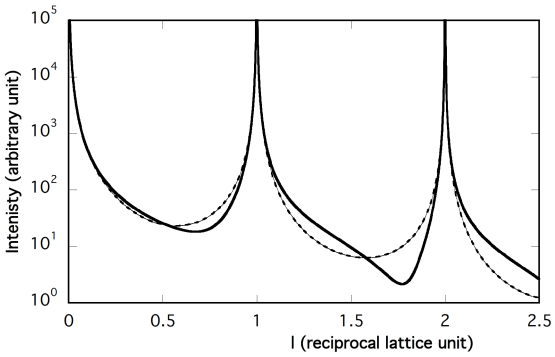


FIG. 1. Intensity distribution along the 00 rod (i.e., the profile along the 00$l$ line) calculated for a simple cubic crystal. The dotted curve is calculated for an ideal perfect crystal (CTR scattering), and the solid curve is for a crystal whose topmost layer is relaxed inward by 5%.

One of the advantages of SXD is that the diffraction process is well described by kinematical theory, that is, only single scattering has to be considered. This has been shown in work based on the dynamical theory of X-ray diffraction[4,7,8], where it was found that the CTR scattering is well approximated by kinematical theory except at positions very close (a few times the Darwin width) to the Bragg point.

As is understood from Eq. (3), the measurement of the integral-order rods gives the three-dimensional surface structure with respect to the substrate crystal. In the case of superstructures formed on the crystal surface, fractional-order rods (FORs) also appear, which give the structure inherent to the superstructure.

SXD in transmission geometry, similar to transmission electron diffraction (TED), is also used to determine the lateral arrangement or to detect a number of diffraction spots simultaneously[9,10].

### C. Reflectivity

The specular reflectivity curve corresponds to the 00 rod profile of the CTR scattering around the region with very small $l(= Q_z)$ values. An important characteristic of the reflectivity measurements is that they do not require any periodicity for the surface structure

or the substrate as long as the surface and interface are sufficiently flat. This makes the specular reflectivity useful for a wide range of structural studies of surfaces and interfaces[11–14]

It is known that the total reflection curve of X-rays from a material with a uniform electron density is equivalent to the Fresnel's curve in optics, and, thus, the exact treatment for surface structure analysis has been well-described by using a recursion formula[15]. Detailed analysis of the reflectivity curve gives information about the depth profile of the electron density at surfaces and interfaces on the nanometer scale.

### D. Instruments for measuring SXD

The conventional method for measuring SXD uses a collimated and monochromatic X-ray beam, and measures the diffracted X-rays sequentially at different sample and detector angles, similar to the X-ray diffraction measurements of bulk crystals. Usually, synchrotron radiation is used because of the weak scattering from surfaces. SXD is different from bulk X-ray diffraction in that the diffracted intensity depends on the experimental geometry, such as the angles of the incident and exit beams to the sample surface[4,16]. The angle between the intensity rod and the major axis of the resolution function also affects the signal intensity. When measuring SXD with standard four-circle diffractometers, these effects must be corrected in the data analysis, or a certain amount of systematic error in the intensities must be accepted. To control these angles, several kinds of multiaxis diffractometers suitable for SXD (six-axis diffractometers are popular) have been developed on the basis of a four-circle diffractometer[17–26]. Angle calculations for the diffractometers and correction factors to evaluate the diffracted intensity $I(\boldsymbol{Q})$ from the observed intensity are given in Refs. 27–32.

Until a few years ago, the intensity at each reciprocal space point was usually obtained by integrating the intensity measured with a point detector during a rotational scan of the sample, with a few exceptions[5]. Recently, two-dimensional detectors have often been used to observe the intensity around a reciprocal space point without rotating the sample, which speeds up the measurement. For time-resolved experiments, methods that are able to simultaneously observe an extended region of reciprocal space have been developed, as explained in Sec. IV. They use an incident X-ray beam with a range of energies and/or incident angles.

Ultrahigh vacuum (UHV) conditions are often essential for surface studies and UHV

chambers have been combined with diffractometers from the beginning of SXD. Although the whole UHV chamber was rotated in early experiments[17], rotary feedthroughs compatible with UHV conditions are usually adopted for sample rotation. A simple practical method is to use a portable baby chamber mountable on a multiaxis diffractometer[33].

### E. Direct methods in SXD

In X-ray diffraction measurements, the intensity of the diffracted X-rays is obtained. Thus, the phase of the diffracted X-ray wave is lost in the measurements. This is known as the phase problem in X-ray diffraction. If one can obtain the phase of the diffracted X-rays, one can reconstruct the electron density distribution of the object by the inverse Fourier transform.

Methods that aim to obtain structural information directly from the measured intensities, without any structural models, are termed as direct methods. The simplest method is the Patterson map[34], which is the Fourier transform of the measured intensities. The result is proportional to the autocorrelation function of the electron density. The peaks in the Patterson map correspond to interatomic vectors. For comparatively simple structures, models can be surmised from the Patterson map, but for more complicated structures, more sophisticated methods that are able to retrieve the phase information are needed.

#### *1. SXD as holography*

Holography is well known as one of the most powerful methods for solving the phase problem in optics. SXD can be interpreted as a holographic process as follows. The total scattering amplitude given by Eq. (2) consists of two waves: $F^{\mathrm{B}}$, the wave diffracted from the bulk crystal whose structure is known, and $F^{\mathrm{S}}$, the wave diffracted from the surface structure whose structure is unknown. The former and the latter can be treated as the reference wave and the object wave in holography, respectively. Thus, the diffracted intensities measured for a number of rods are equivalent to a hologram.

Using the diffracted intensity from the known part $I_0(\boldsymbol{Q}) \equiv |F^{\mathrm{B}}(\boldsymbol{Q})|^2$, the hologram function $\chi(\boldsymbol{Q})$ in SXD can be defined as

$$\chi = \frac{I - I_0}{A} = \frac{|F^{\mathrm{B}} + F^{\mathrm{S}}|^2 - |F^{\mathrm{B}}|^2}{A}, \tag{4}$$

where $A$ is a normalization factor; here, the $\boldsymbol{Q}$ dependence is omitted for visibility. Although the normalization factor is usually defined by $A = I_0$ or $\sqrt{I_0}$ in electron or X-ray fluorescence holography[35], Takahashi et al.[36] adopted $A = F^{\mathrm{B}*}$ as the normalization factor since the diffracted amplitude from the bulk crystal is easily calculated by Eq.(1). Then, the hologram function has the component of the surface structure $F^{\mathrm{S}}$ as

$$\chi = F^{\mathrm{S}} + \frac{F^{\mathrm{B}}}{F^{\mathrm{B}*}} F^{\mathrm{S}*} + \frac{|F^{\mathrm{S}}|^2}{F^{\mathrm{B}*}}. \tag{5}$$

Since the first term of the right-hand side is $F^{\mathrm{S}}$, which has the phase information, we may expect to obtain images of the surface atoms by the inverse Fourier transform of $\chi$. The second term of Eq. (5), corresponding to twin images, might be smeared out and the third term is negligible particularly in the case where $|F^{\mathrm{S}}| < |F^{\mathrm{B}}|$. Thus, the inverse Fourier transform of $\chi$ directly reflects the electron density $\rho(\boldsymbol{r})$ of the surface atoms.

The holographic method was first applied to a monolayer of Ge epitaxially grown on a Si(001)-2×1 surface, and atomic images of Ge were reconstructed three-dimensionally with respect to the Si(001) crystal[37]. This method is also helpful to check whether additional atomic layers exist at the interface[38–40].

### *2. Other model-free phase retrieval methods*

Iterative approaches are a common strategy to solve inverse problems like the phase problem. Fienup has developed an iterative algorithm that involves both the real and Fourier spaces to recover the phases from the intensity data[41,42]. This method is used for coherent X-ray diffractive imaging[43,44].

Saldin and co-workers have applied the algorithm to the analysis of SXD in which the sample lacks periodicity in the direction perpendicular to the sample surface, and succeeded in obtaining images with atomic resolution[45–51].

Figure 2 shows the algorithm. Starting from an appropriate initial electron density $\rho(\boldsymbol{r})$ (for example, flat), the scattering amplitudes $F(\boldsymbol{Q})$ are calculated by a Fourier transform. Only the phases are used and combined with the absolute values from the experiment $|F_{\mathrm{exp}}(\boldsymbol{Q})|$. The scattering amplitudes from the surface region $U(\boldsymbol{Q})$ are calculated by subtracting the scattering amplitudes from the bulk crystal $S(\boldsymbol{Q})$ from the total scattering amplitudes $F(\boldsymbol{Q})$. Next, the real-space electron density of the surface region $\rho'(\boldsymbol{r})$ is calculated

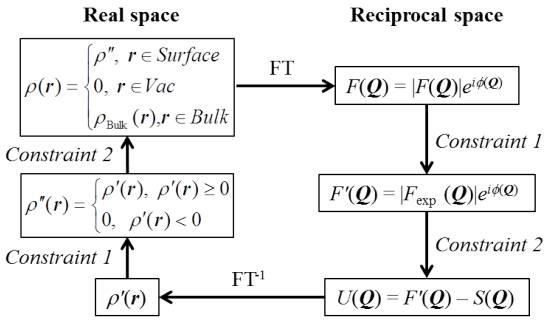


FIG. 2. Schematic drawing of the iterative phase recovery method for surface/interface structures. $S(\boldsymbol{Q})$ is the scattering amplitude from the known part, that is, the bulk crystal, and $U(\boldsymbol{Q})$ is that from the unknown part to be determined.

by the inverse Fourier transform. The electron density is constrained to be non-negative, which yields $\rho''(\boldsymbol{r})$. Then, other constraints specific to SXD are imposed, for example, the electron density should be zero in the vacuum over the surface and equal to the bulk electron density below the surface region. The result is used as the new initial electron density $\rho(\boldsymbol{r})$, and this cycle is repeated until the electron density converges.

Another phase retrieval method, coherent Bragg rod analysis (COBRA), has been developed by Yacoby and co-workers[52–56]. In their method, the phase is semianalytically recovered within the reciprocal space using the scattering amplitude from the known part. In this aspect, COBRA has a similarity with the holographic method.

In both the holography and model-free phase retrieval methods, the structure of the sample surface including the substrate crystal is reconstructed as the three-dimensional electron density distribution. The atomic positions and the magnitude of positional fluctuations are estimated from the electron density distribution.

## III. STATIC STRUCTURE ANALYSES

The structural information of the surface is, similar to the bulk case, essential to obtain physical insight into various surface phenomena. Naturally, the development of the surface structure analysis techniques has commenced from static objects.

The first SXD experiment was performed by Marra et al.[57], who characterized Al thin films epitaxially grown on GaAs(001) substrates using a laboratory X-ray source, and then

investigated the structure of the reconstructed clean surface of Ge(001)-2×1 under UHV conditions using synchrotron radiation[58] . Soon after their work, this technique was applied to the structure analysis of clean surfaces[59–62], adsorbed surfaces[63], and buried interfaces[64] of simple metals and semiconductors to clarify how the surface affects the atomic arrangement (known as surface relaxation and reconstruction). In these studies, mostly in-plane diffraction was used and the Patterson map[34] proved to be effective for determining the two-dimensional surface structures[60,61]. Structural changes accompanying surface melting[65–68], electrodeposition[69], and phase transitions[21,70,71] were also investigated.

Even at this stage, the structure determination of surface reconstructions was a difficult task. Although the in-plane periodicity of the reconstructed surface structure was observed directly, a detailed structure determination sometimes required many years of discussion.

CTR scattering was used by Robinson et al.[72] to obtain information about the structure of the Si(111)-7×7 surface, for which the dimer-adatom-stacking fault (DAS) model had been proposed by Takayanagi et al.[73] from TED experiments. They provided evidence for the stacking faults by the measurements of nonspecular 01 and 10 rods using a sample encapsulated with amorphous Si[72]. Takahashi et al. applied CTR scattering to the structural analysis of the adsorbed surface of Si(111)-$\sqrt{3} \times \sqrt{3}$-Bi. The three-dimensional structure of Bi, with respect to the Si(111) substrate, was determined by measuring the specular rod as well as nonspecular rods[5]. They also proposed a new honeycomb-chained-triangle (HCT) arrangement of Ag atoms in the Si(111)-$\sqrt{3} \times \sqrt{3}$-Ag surface[74], showing that the protrusions observed in scanning tunneling microscopy (STM) images do not always correspond to the atomic sites[75,76]. The CTR scattering was further applied to study the interface structure of an ultrathin $NiSi_2$ film grown on a substrate Si(111) crystal[77]. The early SXD work is summarized in Table 3 of Ref. 3.

Later, samples possessing complex structures were examined. Typical examples are transition-metal oxide surfaces and interfaces. The surface reconstructions of $SrTiO_3$[78,79] and $LaAlO_3$[80], which are typical substrate materials, were reported in the 2000s. Phase transition phenomena in metal oxides have also been studied[81–84], although the detailed real-space structures were not discussed.

As the structure becomes more complex, the difficulty of the intuitive construction of a good structural model increases and becomes practically impossible. Holography and model-free electron density analysis are powerful methods for constructing a good structure model

regardless of the complexity of the bulk structure. In Ref. 85, the authors stressed that the structure refinement of ultrathin films of $LaAlO_3$ can only converged by using the result of holographic analysis (in this case, COBRA) as the starting point for the refinement. There are many other reports on oxide interfaces studied by holographic analyses[55,86,87].

Another example of the application of the holographic technique is the interfacial structure analysis of a Bi(001) thin film epitaxially grown on Si(111)[39], which has a Bi wetting layer at the interface. This explains why the spin splitting expected from the Rashba effect is not observed in the Bi quantum well states[88]. To demonstrate the necessity for model-free electron density analysis, we present two examples of the static structure analysis of surfaces.

### A. Organic semiconductors

Electronic devices based on organic semiconductors have been extensively studied in the past few decades[89]. Organic electroluminescent displays and organic solar cells are already commercially available. The carrier mobility of organic semiconductors is usually studied with field-effect transistors (FETs) made of the organic semiconductors[90–92]. In these devices, carriers move mainly in the vicinity of interfaces[93]. Since the transport properties in organic materials are strongly affected by the molecular arrangements, the surface structure of the organic semiconductors is of importance.

Until 2010, there were no experimental reports on the surface relaxation of organic semiconductors[94]. All the studies on organic semiconductor devices were performed with the assumption that the molecular arrangement is kept unchanged up to the very surface layer with the crystal structure realized deep inside the crystal. The CTR scattering method provides a good picture of the surface relaxation of organic semiconductors. In this case, the unit cell contains too many atoms and the three-dimensional structure is hardly analyzed. Instead, only the depth profile of the electron density is analyzed. For this purpose, only the intensity profile along the $00L$ line (or 00 rod) is required.

Rubrene and tetracene have almost the same highest occupied molecular orbitals (HOMOs), while the carrier mobility of rubrene single crystals is an order of magnitude larger than that of tetracene single crystals. A structural comparison was made on the two materials[95].

The intensity distribution along the 00 rod of tetracene is presented in Fig. 3(a). When

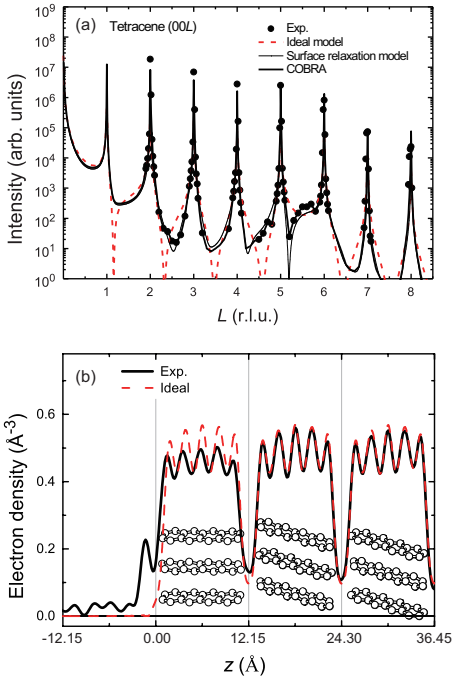


FIG. 3. (Color online) (a) CTR scattering profile of tetracene. (b) Depth profile of the electron density of tetracene single crystal. Figure reproduced from Ref. 95. (c) [2014] Springer Nature.

we assume an ideal surface, that is, a surface with no relaxation, reconstruction, or roughness, the CTR profile drawn by the dashed curve is expected. Since the calculated intensity distribution does not reproduce the experimental results, a large surface relaxation is obvious. COBRA provides the depth profile of the electron density as presented in Fig. 3(b). The electron density profile shows that there are adsorbed molecules on the surface and that the topmost tetracene molecules are rotated by 15° with respect to the bulk. In contrast, no significant surface relaxation was observed for the rubrene surface. For the study of the surface structure of organic materials, COBRA is advantageous because it does not give ghosts in the resulting electron density, unlike the hologram function $\chi$ given in eq. (5). COBRA requires a model structure sufficiently close to the real surface structure. In the case of the organic semiconductor surfaces studied so far, rigid molecular models have been effective in providing the initial model for COBRA.

Based on the experimental results, the band dispersion was examined. In the case of rubrene, which has no surface relaxation, various reports based on the bulk crystal structure[96,97] are valid. For tetracene, the band structure is calculated for the bulk structure and the surface structure[95]. The result shows that the amount of surface relaxation

is sufficiently large to affect the band structure and, therefore, the transport properties at the surface. The result reasonably explains the results of angle-resolved photoelectron spectroscopy on rubrene and tetracene[98]; the former reproduces the theoretical prediction[96], whereas the latter shows severe signal broadening. Very recently, photoelectron spectroscopy results on pentacene were reported[99], and the interpretation of the band structure takes the possible surface relaxation into account.

### B. Si(111)-5x2-Au

One-dimensional chained structures on Si surfaces attract interest because of their electronic properties, such as collective excitation and spin-charge separation[100]. For example, for Si(111) vicinal surfaces, the structures of the Si(557)-Au and Si(553)-Au surfaces have been solved by SXD: a single row of Au is formed on the Si(557) surface[101], while a row of Au dimers is formed on the Si(553) surface[40]. The structure of the Si(111)-$5 \times 2$-Au surface has long been controversial since the discovery of the surface[102], however, because of the complexities arising from the one-dimensional structure in a large unit cell. At the early stage, the coverage of Au was believed to be 0.4 monolayers (ML) and various structural models were proposed on the basis of experimental and theoretical studies[103–105]. Recently, Barke et al. revised the coverage to 0.6 ML by STM studies[106]. Then Erwin et al.[107] proposed a triple Au chain model (EBH model) with a coverage of 0.6 ML by first-principles calculations, revising the previous double chain model[104], while Abukawa and Nishigaya proposed a quite different structural model (AN model) based on Weissenberg reflection high-energy electron diffraction (RHEED) experiments[108]. More recently, Kwon and Kang[109] used first-principles calculations to propose a new model (KK model), shown in Fig. 4(a), with a coverage of 0.7 ML, revising the EBH model by adding another Au atom [marked by **a** in Fig. 4(a)]. The AN model was shown to be inconsistent with optical reflection anisotropy spectroscopy results[110].

Shirasawa et al.[111] have clarified that the KK model agrees best with the SXD experiments. The two-dimensional Patterson map, calculated from 74 fractional-order spot intensities observed in in-plane diffraction measurements, exhibited strong peaks marked by A to F in Fig. 4(b). In general, the interpretation of the Patterson map is not straightforward because of the overlap of interatomic vectors. In the present case, it is natural to consider

that the strong peaks correspond to Au-Au and/or Au-Si interatomic vectors. It was shown by careful analysis that the KK model is favored over the EBH model: for instance, the peak marked by D becomes much weaker in the EBH model. The least-squares fitting analysis performed for the two models, considering only Au atoms, also favored the KK model. The interatomic vectors corresponding to peaks A to F in Fig. 4(b) were finally assigned as shown in Fig. 4(a), where the vectors between Au-Au and Au-Si are illustrated by solid and broken arrows, respectively.

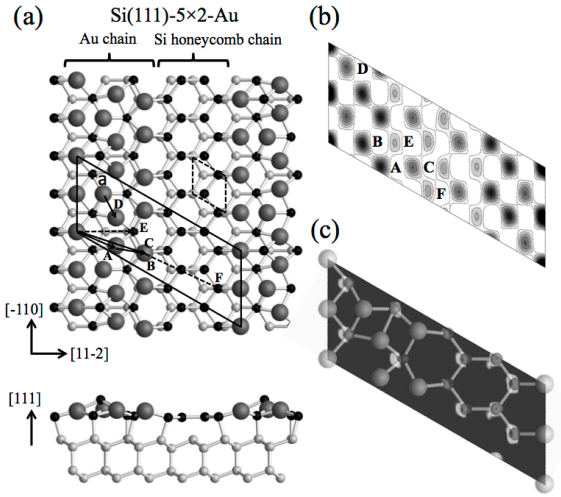


FIG. 4. (a) Structure model of the Si(111)-5×2-Au surface. Large balls indicate Au atoms and small balls indicate Si atoms. (b) Two-dimensional Patterson map calculated from 74 (37 inequivalent) in-plane reflections. Inequivalent peaks A-F are indicated. The corresponding interatomic vectors A-F are indicated in (a) by the solid and broken arrows for Au-Au and Au-Si, respectively. (c) Two-dimensional holographic reconstruction of the reconstructed Si layer. The structure model is overlaid. Figure reproduced from Ref. 111. (c) [2014] American Physical Society

Next, the holographic method was used to obtain the reconstructed Si atoms, using the scattering wave of the known Au atoms as the reference wave. The heavily reconstructed Si atoms, shown as the electron density in Fig. 4(c), were imaged at the Si positions predicted by the theory and were confirmed to form a honeycomb chain structure, as observed in the Si(553)-Au surface[40]. Finally, the three-dimensional structure was determined using the CTR scattering data in addition to the in-plane data, and the result reproduced the KK model well. The reconstructed Si atoms might also be imaged using the well-established

difference Fourier method[60,112]. The present work demonstrates that the holographic method is applicable to in-plane data as well as rod profile data[37–39].

## IV. DYNAMICAL STRUCTURE ANALYSES

According to diffraction theory, the real space structural information is distributed over the whole of the reciprocal space. Thus, to verify the real-space structure model, one needs to have information over a wide range of the reciprocal space. In ordinary diffractometers, however, the intensities are measured sequentially point by point in the reciprocal space. To measure a different point along a rod requires a mechanical movement of the diffractometer. Therefore, the traditional method for time-resolved surface diffraction measurements is to measure the intensity at one specific point in the reciprocal space as a function of time. In this way, the appearance of surface periodicity or roughening of the surface can be monitored.

Time-resolved measurements monitoring a single point in reciprocal space have been performed to investigate crystal growth mechanisms in MBE or CVD processes from the early stage of the SXD[113]. Oscillations in the X-ray intensity during crystal growth, similar to those in RHEED, were observed in the MBE experiments[114] at the anti-Bragg point, where the CTR scattering intensity becomes sensitive to the surface morphology. A review of the recent progress of SXD measurements in MBE systems is given in Ref. 115.

For a further understanding of the dynamic processes at surfaces, it is necessary to simultaneously observe a wide range of the reciprocal space. For the reversible phenomena, the time evolution can be investigated by repeating the experiment many times, each time measuring a different reciprocal space point (this method has a large similarity with the pump-probe method). Recent examples of this kind of measurement are the investigation of electrocrystallization in the underpotential deposition of metals on a Au(111) surface[116] and the observation of the dynamics of the electric double layer of an electrode-ionic liquid interface[117] (see Sect. IV A).

For the irreversible phenomena, the time resolution using standard experimental setups is limited by the time required to scan the angle of the sample and to obtain sufficient statistics. For example, a time resolution of a few minutes was achieved for X-ray reflectivity measurements of liquid surfaces using a high-intensity synchrotron source[118]. Time resolutions below 1 s can be achieved for X-ray reflectivity measurements by performing the

angle scan of the sample as fast as possible[119]. By using high-energy X-rays, Gustafson et al. have recorded several rod profiles at once as the intersections between the rods and a large Ewald sphere in a manner similar to RHEED[120].

A different approach for time-resolved measurements is to use a white X-ray beam at a fixed incident angle in combination with an energy-resolving detector[121–125]. In this way, the momentum transfer range corresponding to the energy range of the incident beam can be observed simultaneously. This method has mainly been applied to X-ray reflectivity measurements, for example, an in operando study of an organic solar cell[126] and an investigation of the growth of organic thin films[127]. A review of the energy-dispersive method has also been published[128].

Simultaneous measurement of the scattering profile in a momentum range is also possible by using a monochromatic X-ray beam that has a range of incident angles onto the sample and measuring the scattered X-rays with a one-dimensional or two-dimensional detector. This has been used for measuring the X-ray reflectivity by Naudon et al.[129] and other authors[130–132]. The same idea can also be applied to CTR scattering from multilayer structures[133–135]. These methods are best suited to laboratory X-ray sources but provide too weak an intensity for measurements with atomic resolution.

Recently developed photon-counting two-dimensional detectors[136] combined with state-of-the-art X-ray optics and synchrotron sources have made it possible to implement a method with improved accuracy and time resolution and to extend the measurement to atomic resolution. This simultaneous multiwavelength dispersive diffractometer uses a curved crystal polychromator to create a fan-shaped convergent beam, for which the wavelength changes along the cross section of the beam (Fig. 5). The sample is placed at the focus of the beam. To measure CTR profiles, the diffracted X-rays for a fixed angle between the incident beam and the diffracting plane of the sample are observed with a position-sensitive detector, giving the CTR profile in the momentum range corresponding to the wavelength range of the incident beam[137]. Reflected intensities corresponding to one atomic layer can be observed in 1 s.

To measurie a wide part of the reflectivity profile, it is advantageous to use not only a range of wavelengths but also a range of incident angles onto the sample. This can be achieved by inclining the sample with respect to the X-ray beam. It has been shown that an X-ray reflectivity curve can be measured in 10 ms with this approach[138]. By using a bent-

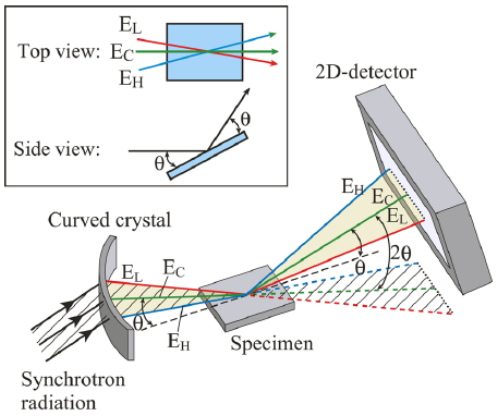


FIG. 5. (Color online) X-ray optical layout of the simultaneous multiwavelength dispersive diffractometer for time-resolved CTR measurements. An example of research using this method is presented in Sect. IV B. Figure reproduced from Ref. 137. (c) [2011] AIP Publishing.

twisted crystal polychromator, it is possible to keep the sample horizontal and incline the X-ray beam with respect to the sample[139,140]. This has been used to observe the adsorption of proteins on a liquid surface[141].

Here, we present two recent time-resolved SXD studies. One is the time evolution of an electric double layer (EDL) measured with the ordinary method. The other is the photoinduced water wettability transition of $TiO_2$ measured with the novel simultaneous multiwavelength dispersive diffractometer.

### A. Electric double layer at an ionic liquid/Au interface

The liquid structure around solid-liquid interfaces is one of the less-understood frontiers, although it is the entity of EDLs, the scene of chemical reactions, and the origin of the electricity provided by batteries. Ionic liquids (ILs), which are salts whose melting point is lower than 100 °C, are the concentrated limit of the electrolyte in a naive description. According to the Gouy–Chapman model of the EDL, the thickness of the EDL is proportional to $n^{-1/2}$, where $n$ is the ion density. Therefore, ionic liquids should have an extremely thin EDL, which produces a huge electric field at the interface that leads to various applications[142–147]. However, theoretical models of EDLs were developed for simple dilute solutions, which is a very different situation from ionic liquids. Experimental observation of the detailed structure of

IL-EDLs is therefore necessary to understand ionic liquids[148,149].

Highly charged EDLs are often understood on the basis of the Gouy–Chapman–Stern model, which is a combination of the Helmholtz model ($\sim$1 nm from the interface) and the Gouy–Chapman model ($\sim$1 $\mu$m from the interface). In the Helmholtz layers, "liquid ions" strongly adsorbed on the solid surface have only small positional fluctuations and can be understood as a part of the solid side[150–152].

In the case of IL-EDLs, layered structures were observed by X-ray reflectivity measurements on an IL-sapphire interface[153] and by AFM on an IL-gold interface[154]. The first non-contact measurement of the IL-EDL structure with controlled electric potential was reported in Ref. 155 for a Au (111) and N,N-diethyl-N-methyl-N-(2-methoxyethyl)ammonium-bis(trifluoromethanesulfonyl)imide (DEME-TFSI) interface. The time evolution of the same interface was recently reported in Ref. 156, and the EDL structures of some other ILs have been reported in recent years[117,157,158].

The reflectivity profiles measured at a positively charged Au (111) surface immersed in an IL were found to be modulated from those at a negatively charged surface. The change in intensity caused by the applied voltage $(I^+ - I^-)/(I^+ + I^-)$, where $I^\pm$ denotes the intensity measured at the positively/negatively charged Au surface, is presented in Fig. 6(a). The structural model for the EDL was chosen to reproduce the $(I^+ - I^-)/(I^+ + I^-)$ profile. The real space structure of the IL-EDL is presented in Fig. 6(b). As can be seen, the layered liquid structure is very different for the positive and negative electric potentials.

The time evolution of the IL-EDL has been studied through electrochemical measurements[159–162]. It is well known that the time evolution has fast and slow components, whose time constants are $\sim$1 ms and $\sim$10 s, respectively. The microscopic origin of the time evolution is often studied through molecular dynamics (MD) calculations, and several MD calculation works on the IL-EDL have been published[163–165]. However, such calculations can cover a timescale of only up to $\sim$50 ns. There is a huge gap between the computationally accessible and experimentally observed timescales. SXD can provide microscopic information of the IL-EDL as a function of time with an appropriate timescale.

Reference 157 reports the time evolution of the reflectivity from an IL-EDL at $q$ =0.3 Å$^{-1}$ just after potential switching. Figure 7(a) presents the results. As can be seen, both $-0.4$ to 1.0 V and 1.0 to $-0.4$ V switchings cause structural changes with very fast and slow components, whose time constants are less than 1 and $\simeq$10 s, respectively. The slow time

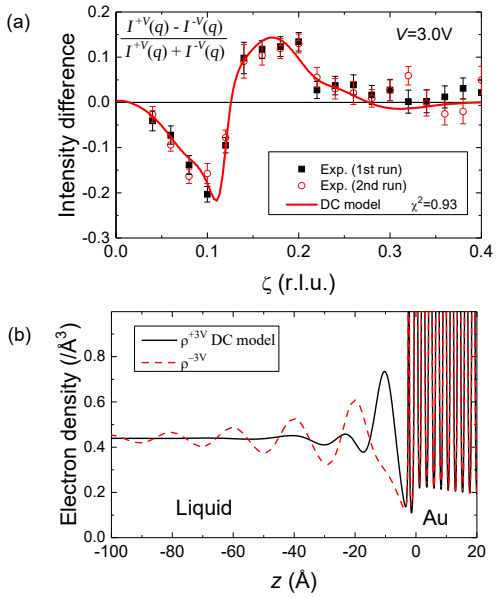


FIG. 6. (Color online) (a) Change in scattering intensity caused by the external voltage. (b) Real-space electron density profile of the IL-EDL. Figure reproduced from Ref. 155. (c) [2012] AIP Publishing.

constant is much slower than the time constant of the circuit, and, therefore, the slow dynamics is intrinsic.

Reference 117 reports the time dependence of the reflectivity in a finite range of the scattering vector $q$ as shown in Fig. 7(b). The measurements were performed during potential cycling between $-0.4$ and $+1.0$ V at 100 mVs$^{-1}$. The reflectivity $R$ as a function of $q$ at potential $V$ is reproduced well by the function

$$R(q, V) = n(V)R_{\mathrm{N}}(q) + [1 - n(V)]R_{\mathrm{P}}(q), \tag{6}$$

where $R_{\mathrm{N}}$ and $R_{\mathrm{P}}$ denote the reflectivity at extreme negative ($-0.4$ V) and positive ($+1.0$ V) potentials, respectively. The results of the fitting are presented in Fig. 7(c) with the value of $n(V)$ plotted in Fig. 7(d). This successful fitting to Eq. (6) was interpreted as a sign of a bistable interfacial structure, that is, the electron density of the IL at potential $V$ can be expressed as

$$\rho(V, z) = n(V)\rho_{\mathrm{N}}(z) + [1 - n(V)]\rho_{\mathrm{P}}(z), \tag{7}$$

where $z$ is the distance from the electrode surface, and $\rho_{\mathrm{N}}(z)$ and $\rho_{\mathrm{P}}(z)$ denote the electron density at extreme negative ($-0.4$ V) and positive ($+1.0$ V) potentials, respectively.

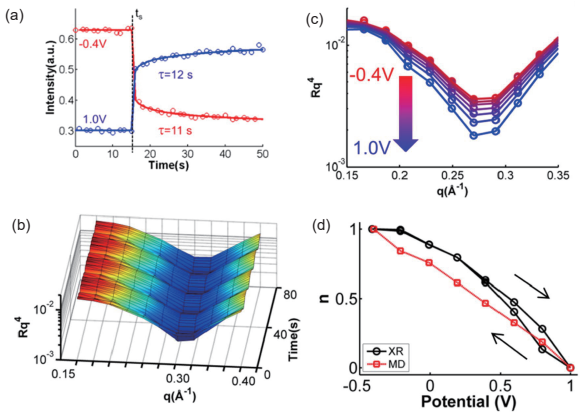


FIG. 7. (Color online) (a) Time dependence of the X-ray reflectivity at $q$ =0.3 Å$^{-1}$ with potential switching from −0.4 to 1.0 V (red) and 1.0 to −0.4 V (blue), whose time constants are 11 and 12 s, respectively. Reprinted with permission from Ref. 157. Copyright 2014 American Chemical Society. (b) Reflectivity $R(q,t)$ multiplied by $q^4$ as a function of $q$ and time during potential cycling at 100 mVs$^{-1}$. (c) Potential-dependent intensity (symbols) as a function of $q$. The lines show the best fits to Eq. (6). (d) Potential-dependent weighting factor $n$ obtained by fitting to Eq. (6) (black circles) and MD simulations (red squares). Reprinted with permission from Ref. 117. Copyright 2015 IOP Publishing.

The electron density described by Eq. (7) is well reproduced by MD simulations[117], while the time evolution derived in MD is much quicker than the experimental results. A total understanding of the IL-EDL requires a breakthrough in the theoretical modeling.

### B. Photoinduced water wettability transition of rutile-$TiO_2$(110) surface

A hydrophobic $TiO_2$ surface can be converted to a hydrophilic surface by irradiation with UV light with an energy greater than the bandgap of 3 eV [Fig. 8(a)]. The water wettability transition was discovered in the late 1990s[166,167]. This photochemical property extends the range of applications of the representative photocatalytic material to, for instance, anti-fog, self-cleaning, and heat-dissipation coatings[168,169]. Despite a number of studies devoted to understanding the underlying atomic-scale processes, controversy remains with regards to the mechanism. In particular, it is still not clear whether and how the surface structure is involved. Several groups have claimed that the photocatalytic decomposition of hydrophobic surface impurities results in the hydrophilicity[170–175]. Other groups have claimed that a

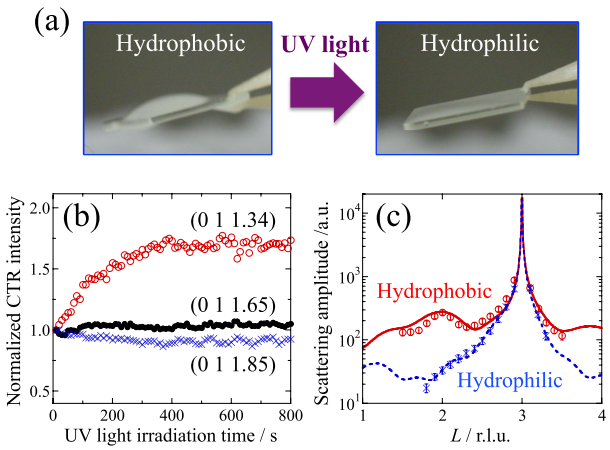


FIG. 8. (Color online) (a) Photoinduced hydrophobic-hydrophilic transition of the rutile-$TiO_2$(110) surface. (b) Time evolution of the CTR scattering intensity in the (01$L$) rod during UV light ($\lambda = 365$ nm, 87 mW/cm$^2$) irradiation. (c) Measured (symbols) and calculated (solid and dashed lines) CTR scattering profiles of the (10$L$) rod of the hydrophobic and hydrophilic rutile-$TiO_2$(110) surfaces. Figure reproduced from Ref. 185. (c) [2016] ACS Publications.

photoinduced structural change of the $TiO_2$ surface leads to the hydrophilicity[169,176–181]. The controversy at least partly arises from the difficulty in observing the atomic-scale processes during the wettability transition. Conventional surface science techniques operatable in a vacuum are often inadequate for studying the phenomenon because the surface processes in a vacuum are different from those under ambient conditions. Furthermore, it is known that the hydrophilic state is a metastable state and rapidly recovers to the hydrophobic state in a vacuum[182]. Theoretical studies are also challenging because the energy hierarchy for the water adsorption phases varies according to the calculation conditions[183,184]. Therefore, in-situ SXD observations of the interface processes are useful for understanding the atomic-scale processes occurring during the transition.

Time-resolved CTR scattering measurements in the energy-dispersive mode[137] (see Fig. 5) demonstrated the occurrence of structural change during UV light irradiation on a rutile-$TiO_2$(110) surface under a humid condition[185]. Figure 8(b) shows the time evolution of the CTR scattering intensity at different positions on the (01$L$) rod during UV light ($\lambda = 365$ nm, 87 mW/cm$^2$) irradiation. The changes in intensity are finished within about 300 s. The time scale is the same as that of the wettability transition[176], indicating that a structural change is associated with the wettability transition. No change in intensity was observed

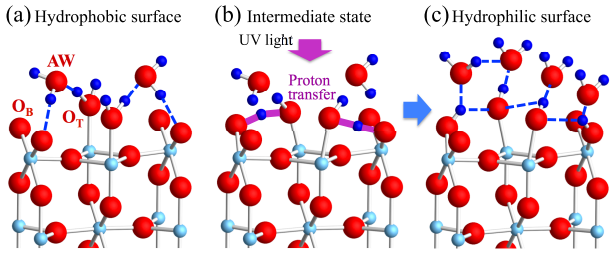


FIG. 9. (Color online) (a) Mechanism of the photoinduced wettability transition of a rutile-$TiO_2$(110) surface, proposed on the basis of a CTR study[185]. Oxygen, titanium, and hydrogen atoms are respectively represented as large, medium, and small balls. Hydrogen bonds are represented as dashed lines in (a) and (c), and the proton transfer is indicated by the bold lines in (b). Figure reproduced from Ref. 185. (c) [2016] ACS Publications.

when the UV light power was lower than 20 mW/cm$^2$, which is consistent with the power threshold for the wettability transition[176].

The structures of the hydrophobic and hydrophilic surfaces were revealed by quantitative structural analysis on the static CTR data. The CTRs were drastically changed upon photoirradiation, as shown in Fig. 8(c). On the hydrophobic surface, the determined structure indicates that the five-coordinated Ti atom is terminated with an O atom [denoted as $O_T$ in Fig. 9(a)], likely to be in the form of a water molecule, the surface bridging O atoms [denoted as $O_B$ in Fig. 9(a)] are not hydroxylated, and the surface is covered with a small amount of O atoms (site occupancy is $\sim 0.3$), likely in the form of a water molecule located at a lattice site [denoted as AW in Fig. 9(a)][185]. The results are consistent with the previous CTR study on the surface in water[186] and theoretical studies[183,187]. On the hydrophilic surface, large positional fluctuations are found for the $O_T$, $O_B$, and the topmost TiO layer, and the structured AW layer is no longer seen in the diffraction data.

The structural change can be interpreted, in terms of the water wettability transition, as being caused by photoinduced proton transfer from the intact water at the $O_T$ site to the non-hydroxylated oxygen at the $O_B$ site[188] [Fig. 9(b)]. The resulting surface OH group at the $O_T$ and $O_B$ sites can be active sites for water adsorption [Fig. 9(c)]. The neighboring OH groups at the $O_T$ and $O_B$ sites can form a hydrogen bond with each other, which results in the large positional displacement[189]. The displacement is expected to cause a local lattice strain in the underlying $TiO_2$ layers. These might appear as the large lateral positional fluctuation of the $O_T$, $O_B$, and the topmost TiO layer as observed in the CTR study. The adsorbed water

molecules on the surface might be more disordered and invisible in the diffraction data. It is known that the hydrophilic surface consists of hydrophobic and hydrophilic domains and that these domains are limited in size to several tens of nanometers[166,167]. The domain size limitation might be related to the lattice strain induced by the hydrogen-bond formation. Note that on the hydrophilic surface, the CTR study provides the average information over the coexisting hydrophobic and hydrophilic domains since the X-ray beam size on the order of 0.1 mm is much larger than the domain size. Experiments with an X-ray beam having a few nm diameter would provide a deeper understanding of the wettability transition.

## V. SUMMARY

In this review article, we have summarized the 30 years of history of surface X-ray diffraction. The weak interaction between X-rays and matter has been regarded as a disadvantage for surface studies. However, the development of intense X-ray sources and efficient X-ray detectors has overcome this disadvantage. Now, the weak interaction is rather a merit of the X-rays that allows us to perform quantitative data analysis as well as to study the buried interfaces. Despite the notorious variety of surface/interface structures, static structures can be analyzed by model-free phase retrieval analyses. The dynamic structure at the interface is also of importance because the interfaces are where the chemical reactions proceed. Time-dependent SXD experiments are now developing, and two recent examples have been discussed.

The recent trend of the upgrade plans of synchrotron facilities aims to provide bright coherent X-rays. By using coherent X-rays for SXD, one can study the dynamics at a surface and interface at a time scale of ms to h and a length scale of a few nanometers[115,190,191]. Together with the combination of a new analysis method based on informatics, the surface X-ray diffraction technique provides a better understanding of surfaces, interfaces, and nanostructures with useful functionality.

## ACKNOWLEDGMENTS

This work was supported by Grants-in-Aid for Scientific Research (JSPS KAKENHI, Grant Nos. JP26105008, JP24760542, JP26287080, 15H01044) and by JST, PRESTO.

The development of the time-resolved surface diffractometer was supported by the program 'Development of Advanced Measurement and Analysis Systems' of the Japan Science and Technology Agency. The synchrotron radiation experiments at the Photon Factory were performed with the approval of the Photon Factory Program Advisory Committee (Proposal Nos. 2005G135, 2008G083, 2010G012, 2011G068, 2013S2-001, 2014G152, and 2015S2-009). The synchrotron radiation experiments at beamline BL13XU of SPring-8 were performed with the approval of the Japan Synchrotron Radiation Research Institute (JASRI) (Proposal Nos. 2010B1739, 2011A1625, 2011B1726).

---

[1] S. Andrews and R. Cowley: Journal of Physics C: Solid State Physics **18** (1985) 6427.

[2] I. Robinson: Physical Review B **33** (1986) 3830.

[3] R. Feidenhans'l: Surface Science Reports **10** (1989) 105.

[4] T. Takahashi and S. Nakatani: Surface Science **326** (1995) 347.

[5] T. Takahashi, S. Nakatani, T. Ishikawa, and S. Kikuta: Surface Science **191** (1987) L825 .

[6] E. Vlieg, J. Van Der Veen, S. Gurman, C. Norris, and J. Macdonald: Surface Science **210** (1989) 301.

[7] A. Caticha: Phys. Rev. B **47** (1993) 76.

[8] S. Nakatani and T. Takahashi: Surface Science **311** (1994) 433.

[9] T. Takahashi, S. Nakatani, N. Okamoto, T. Ishikawa, and S. Kikuta: Surface Science **242** (1991) 54.

[10] H. Tajiri, O. Sakata, and T. Takahashi: Applied Surface Science **234** (2004) 403.

[11] T. Russell: Materials Science Reports **5** (1990) 171.

[12] J. Als-Nielsen: *Handbook on Synchrotron Radiation. Vol. 3*, ed. G. Brown and D. E. Moncton (Elsevier, Amsterdam, 1991) Chapter 12.

[13] J. Als-Nielsen, D. Jacquemain, K. Kjaer, F. Leveiller, M. Lahav, and L. Leiserowitz: Physics Reports **246** (1994) 251.

[14] J. Daillant and A. Gibaud (ed.): *X-ray and Neutron Reflectivity* (Springer, Berlin Heidelberg, 2009)

[15] L. Parratt: Physical Review **95** (1954) 359.

[16] W. Yashiro and T. Takahashi: Acta Crystallographica Section A: Foundations of Crystallography **56** (2000) 163.

[17] S. Brennan and P. Eisenberger: Nuclear Instruments and Methods In Physics Research **222** (1984) 164.

[18] P. Fuoss and I. Robinson: Nuclear Instruments and Methods In Physics Research **222** (1984) 171.

[19] E. Vlieg, A. Van 't Ent, A. De Jongh, H. Neerings, and J. Van Der Veen: Nuclear Inst. and Methods in Physics Research, A **262** (1987) 522.

[20] K. Akimoto, J. Mizuki, I. Hirosawa, and J. Matsui: Review of Scientific Instruments **60** (1989) 2362.

[21] D. Gibbs, B. Ocko, D. Zehner, and S. Mochrie: Physical Review B **42** (1990) 7330.

[22] G. Renaud, B. Villette, and P. Guenard: Nuclear Inst. and Methods in Physics Research, B **95** (1995) 422.

[23] S. Ferrer and F. Comin: Review of Scientific Instruments **66** (1995) 1674.

[24] M. Takahasi, S. Nakatani, Y. Ito, T. Takahashi, X. Zhang, and M. Ando: Surface Science **357-358** (1996) 78.

[25] M. Takahasi, Y. Yoneda, H. Inoue, N. Yamamoto, and J. Mizuki: Japanese Journal of Applied Physics, Part 1: Regular Papers and Short Notes and Review Papers **41** (2002) 6247.

[26] O. Sakata, Y. Furukawa, S. Goto, T. Mochizuki, T. Uruga, K. Takeshita, H. Ohashi, T. Ohata, T. Matsushita, S. Takahashi, H. Tajiri, T. Ishikawa, M. Nakamura, M. Ito, K. Sumitani, T. Takahashi, T. Shimura, A. Saito, and M. Takahasi: Surface Review and Letters **10** (2003) 543.

[27] J. M. Bloch: Journal of Applied Crystallography **18** (1985) 33.

[28] M. Lohmeier and E. Vlieg: Journal of Applied Crystallography **26** (1993) 706.

[29] K. W. Evans-Lutterodt and M. T. Tang: Journal of Applied Crystallography **28** (1995) 318.

[30] E. Vlieg: Journal of Applied Crystallography **30** (1997) 532.

[31] E. Vlieg: Journal of Applied Crystallography **31** (1998) 198.

[32] H. You: Journal of Applied Crystallography **32** (1999) 614.

[33] T. Slobodskyy, P. Schroth, D. Grigoriev, A. Minkevich, D. Hu, D. Schaadt, and T. Baumbach: Review of Scientific Instruments **83** (2012) 105112.

[34] B. E. Warren: *X-ray Diffraction* (Addison-Wesley, Reading, MA, 1969)

[35] J. Barton: Physical Review Letters **67** (1991) 3106.

[36] T. Takahashi, K. Sumitani, and S. Kusano: Surface Science **493** (2001) 36.

[37] K. Sumitani, T. Takahashi, S. Nakatani, A. Nojima, O. Sakata, Y. Yoda, S. Koh, T. Irisawa, and Y. Shiraki: Japanese Journal of Applied Physics, Part 2: Letters **42** (2003) L189.

[38] T. Takahashi, T. Shirasawa, K. Sekiguchi, and W. Voegeli: e-Journal of Surface Science and Nanotechnology **7** (2009) 525.

[39] T. Shirasawa, M. Ohyama, W. Voegeli, and T. Takahashi: Phys. Rev. B **84** (2011) 075411.

[40] W. Voegeli, T. Takayama, T. Shirasawa, M. Abe, K. Kubo, T. Takahashi, K. Akimoto, and H. Sugiyama: Phys. Rev. B **82** (2010) 075426.

[41] D. Sayre: Acta Crystallographica **5** (1952) 843.

[42] J. Fienup: Optics Letters **3** (1978) 27.

[43] J. Miao, P. Charalambous, J. Kirz, and D. Sayre: Nature **400** (1999) 342.

[44] J. Miao, T. Ishikawa, Q. Shen, and T. Earnest: Annual Review of Physical Chemistry **59** (2008) 387.

[45] D. Saldin, R. Harder, H. Vogler, W. Moritz, and I. Robinson: Computer Physics Communications **137** (2001) 12.

[46] D. Saldin, R. Harder, V. Shneerson, and W. Moritz: Journal of Physics Condensed Matter **13** (2001) 10689.

[47] D. Saldin, V. Shneerson, and R. Fung: Physica B: Condensed Matter **336** (2003) 16.

[48] P. Lyman, V. Shneerson, R. Fung, R. Harder, E. Lu, S. Parihar, and D. Saldin: Physical Review B - Condensed Matter and Materials Physics **71** (2005) 081402.

[49] P. Lyman, V. Shneerson, R. Fung, S. Parihar, H. Johnson-Steigelman, E. Lu, and D. Saldin: Surface Science **600** (2006) 424.

[50] R. Fung, V. Shneerson, P. Lyman, S. Parihar, H. Johnson-Steigelman, and D. Saldin: Acta Crystallographica Section A: Foundations of Crystallography **63** (2007) 239.

[51] D. Saldin and V. Shneerson: Journal of Physics Condensed Matter **20** (2008) 304208.

[52] Y. Yacoby, R. Pindak, R. MacHarrie, L. Pfeiffer, L. Berman, and R. Clarke: Journal of Physics Condensed Matter **12** (2000) 3929.

[53] Y. Yacoby, M. Sowwan, E. Stern, J. Cross, D. Brewe, R. Pindak, J. Pitney, E. Dufresne, and R. Clarke: Nature Materials **1** (2002) 99.

[54] M. Sowwan, Y. Yacoby, J. Pitney, R. MacHarrie, M. Hong, J. Cross, D. Walko, R. Clarke, R. Pindak, and E. Stern: Physical Review B - Condensed Matter and Materials Physics **66**

(2002) .

[55] D. D. Fong, C. Cionca, Y. Yacoby, G. B. Stephenson, J. A. Eastman, P. H. Fuoss, S. K. Streiffer, C. Thompson, R. Clarke, R. Pindak, and E. A. Stern: Phys. Rev. B **71** (2005) 144112.

[56] D. Kumah, S. Shusterman, Y. Paltiel, Y. Yacoby, and R. Clarke: Nature Nanotechnology **4** (2009) 835.

[57] W. Marra, P. Eisenberger, and A. Cho: Journal of Applied Physics **50** (1979) 6927.

[58] P. Eisenberger and W. Marra: Physical Review Letters **46** (1981) 1081.

[59] I. Robinson: Physical Review Letters **50** (1983) 1145.

[60] J. Bohr, R. Feidenhans'l, M. Nielsen, M. Toney, R. L. Johnson, and I. K. Robinson: Phys. Rev. Lett. **54** (1985) 1275.

[61] I. K. Robinson, W. K. Waskiewicz, P. H. Fuoss, J. B. Stark, and P. A. Bennett: Phys. Rev. B **33** (1986) 7013.

[62] A. R. Sandy, S. G. J. Mochrie, D. M. Zehner, K. G. Huang, and D. Gibbs: Phys. Rev. B **43** (1991) 4667.

[63] E. Vlieg, A. V. D. Gon, J. V. D. Veen, J. MacDonald, and C. Norris: Surface Science **209** (1989) 100.

[64] K. Akimoto, I. Hirosawa, J. Mizuki, S. Fujieda, Y. Matsumoto, and J. Matsui: Japanese Journal of Applied Physics **27** (1988) L1401.

[65] W. C. Marra, P. H. Fuoss, and P. E. Eisenberger: Phys. Rev. Lett. **49** (1982) 1169.

[66] S. Brennan, P. H. Fuoss, and P. Eisenberger: Phys. Rev. B **33** (1986) 3678.

[67] G. A. Held, J. L. Jordan-Sweet, P. M. Horn, A. Mak, and R. J. Birgeneau: Phys. Rev. Lett. **59** (1987) 2075.

[68] P. H. Fuoss, L. J. Norton, and S. Brennan: Phys. Rev. Lett. **60** (1988) 2046.

[69] M. G. Samant, M. F. Toney, G. L. Borges, L. Blum, and O. R. Melroy: Surface Science **193** (1988) L29.

[70] H. Dosch, L. Mailänder, A. Lied, J. Peisl, F. Grey, R. L. Johnson, and S. Krummacher: Phys. Rev. Lett. **60** (1988) 2382.

[71] I. Robinson, A. MacDowell, M. Altman, P. Estrup, K. Evans-Lutterodt, J. Brock, and R. Birgeneau: Physical Review Letters **62** (1989) 1294.

[72] I. K. Robinson, W. K. Waskiewicz, R. T. Tung, and J. Bohr: Phys. Rev. Lett. **57** (1986) 2714.

[73] K. Takayanagi, Y. Tanishiro, S. Takahashi, and M. Takahashi: Surface Science **164** (1985) 367 .

[74] T. Takahashi, S. Nakatani, N. Okamoto, T. Ishikawa, and S. Kikuta: Japanese Journal of Applied Physics **27** (1988) L753.

[75] R. Wilson and S. Chiang: Physical Review Letters **58** (1987) 369.

[76] E. Van Loenen, J. Demuth, R. Tromp, and R. Hamers: Physical Review Letters **58** (1987) 373.

[77] I. Robinson, R. Tung, and R. Feidenhans'l: Physical Review B **38** (1988) 3632.

[78] G. Charlton, S. Brennan, C. Muryn, R. McGrath, D. Norman, T. Turner, and G. Thornton: Surface Science **457** (2000) L376.

[79] R. Herger, P. R. Willmott, O. Bunk, C. M. Schlepütz, B. D. Patterson, B. Delley, V. L. Shneerson, P. F. Lyman, and D. K. Saldin: Phys. Rev. B **76** (2007) 195435.

[80] R. J. Francis, S. C. Moss, and A. J. Jacobson: Phys. Rev. B **64** (2001) 235425.

[81] G. M. Watson, D. Gibbs, G. H. Lander, B. D. Gaulin, L. E. Berman, H. Matzke, and W. Ellis: Phys. Rev. Lett. **77** (1996) 751.

[82] G. M. Watson, D. Gibbs, G. H. Lander, B. D. Gaulin, L. E. Berman, H. Matzke, and W. Ellis: Phys. Rev. B **61** (2000) 8966.

[83] Y. Wakabayashi, M. Upton, S. Grenier, J. Hill, C. Nelson, J.-W. Kim, P. Ryan, A. Goldman, H. Zheng, and J. Mitchell: Nature Materials **6** (2007) 972.

[84] S. Wilkins, X. Liu, Y. Wakabayashi, J.-W. Kim, P. Ryan, H. Zheng, J. Mitchell, and J. Hill: Physical Review B - Condensed Matter and Materials Physics **84** (2011) 165103.

[85] P. Willmott, S. Pauli, R. Herger, C. Schlepütz, D. Martoccia, B. Patterson, B. Delley, R. Clarke, D. Kumah, C. Cionca, and Y. Yacoby: Physical Review Letters **99** (2007) 155502.

[86] R. Yamamoto, C. Bell, Y. Hikita, H. Hwang, H. Nakamura, T. Kimura, and Y. Wakabayashi: Physical Review Letters **107** (2011) 036104.

[87] T. Fister, H. Zhou, Z. Luo, S. Seo, S. Hruszkewycz, D. Proffit, J. Eastman, P. Fuoss, P. Baldo, H. Lee, and D. Fong: APL Materials **2** (2014) 021102.

[88] A. Takayama, T. Sato, S. Souma, T. Oguchi, and T. Takahashi: Nano Letters **12** (2012) 1776.

[89] H. Klauk: *Organic Electronics: Materials, Manufacturing and Applications* (Wiley-VCH, New Jersey, 2006)

[90] V. Butko, X. Chi, and A. Ramirez: Solid State Communications **128** (2003) 431.

[91] R. De Boer, T. Klapwijk, and A. Morpurgo: Applied Physics Letters **83** (2003) 4345.

[92] C. Reese, W.-J. Chung, M.-M. Ling, M. Roberts, and Z. Bao: Applied Physics Letters **89** (2006) 202108.

[93] J. Takeya, M. Yamagishi, Y. Tominari, R. Hirahara, Y. Nakazawa, T. Nishikawa, T. Kawase, T. Shimoda, and S. Ogawa: Applied Physics Letters **90** (2007) 102120.

[94] Y. Wakabayashi, J. Takeya, and T. Kimura: Phys. Rev. Lett. **104** (2010) 066103.

[95] H. Morisaki, T. Koretsune, C. Hotta, J. Takeya, T. Kimura, and Y. Wakabayashi: Nature Communications **5** (2014) 5400.

[96] D. Da Silva Filho, E.-G. Kim, and J.-L. Brédas: Advanced Materials **17** (2005) 1072.

[97] S. Yanagisawa, Y. Morikawa, and A. Schindlmayr: Phys. Rev. B **88** (2013) 115438.

[98] A. Vollmer, R. Ovsyannikov, M. Gorgoi, S. Krause, M. Oehzelt, A. Lindblad, N. Mårtensson, S. Svensson, P. Karlsson, M. Lundvuist, T. Schmeiler, J. Pflaum, and N. Koch: Journal of Electron Spectroscopy and Related Phenomena **185** (2012) 55.

[99] Y. Nakayama, Y. Mizuno, M. Hikasa, M. Yamamoto, M. Matsunami, S. Ideta, K. Tanaka, H. Ishii, and N. Ueno: Journal of Physical Chemistry Letters **8** (2017) 1259.

[100] J. Crain and F. Himpsel: Applied Physics A **82** (2006) 431.

[101] I. K. Robinson, P. A. Bennett, and F. J. Himpsel: Phys. Rev. Lett. **88** (2002) 096104.

[102] H. E. Bishop and J. C. Riviére: Journal of Physics D: Applied Physics **2** (1969) 1635.

[103] L. D. Marks and R. Plass: Phys. Rev. Lett. **75** (1995) 2172.

[104] S. C. Erwin: Phys. Rev. Lett. **91** (2003) 206101.

[105] C.-Y. Ren, S.-F. Tsay, and F.-C. Chuang: Phys. Rev. B **76** (2007) 075414.

[106] I. Barke, F. Zheng, S. Bockenhauer, K. Sell, V. v. Oeynhausen, K. H. Meiwes-Broer, S. C. Erwin, and F. J. Himpsel: Phys. Rev. B **79** (2009) 155301.

[107] S. C. Erwin, I. Barke, and F. J. Himpsel: Phys. Rev. B **80** (2009) 155409.

[108] T. Abukawa and Y. Nishigaya: Phys. Rev. Lett. **110** (2013) 036102.

[109] S. G. Kwon and M. H. Kang: Phys. Rev. Lett. **113** (2014) 086101.

[110] C. Hogan, E. Ferraro, N. McAlinden, and J. F. McGilp: Phys. Rev. Lett. **111** (2013) 087401.

[111] T. Shirasawa, W. Voegeli, T. Nojima, Y. Iwasawa, Y. Yamaguchi, and T. Takahashi: Phys. Rev. Lett. **113** (2014) 165501.

[112] M. Nakamura and M. Ito: Phys. Rev. Lett. **94** (2005) 035501.

[113] P. H. Fuoss, D. W. Kisker, G. Renaud, K. L. Tokuda, S. Brennan, and J. L. Kahn: Phys. Rev. Lett. **63** (1989) 2389.

[114] E. Vlieg, A. Van Der Gon, J. Van Der Veen, J. MacDonald, and C. Norris: Physical Review Letters **61** (1988) 2241.

[115] M. Takahasi: Journal of the Physical Society of Japan **82** (2013) 021011.

[116] M. Nakamura, T. Banzai, Y. Maehata, O. Endo, H. Tajiri, O. Sakata, and N. Hoshi: Scientific Reports **7** (2017) 914.

[117] A. Uysal, H. Zhou, G. Feng, S. Lee, S. Li, P. Cummings, P. Fulvio, S. Dai, J. McDonough, Y. Gogotsi, and P. Fenter: Journal of Physics Condensed Matter **27** (2015) 032101.

[118] Y. Yano, T. Uruga, H. Tanida, H. Toyokawa, Y. Terada, and H. Yamada: Journal of Synchrotron Radiation **17** (2010) 511.

[119] M. Lippmann, A. Buffet, K. Pflaum, A. Ehnes, A. Ciobanu, and O. Seeck: Review of Scientific Instruments **87** (2016) 113904.

[120] J. Gustafson, M. Shipilin, C. Zhang, A. Stierle, U. Hejral, U. Ruett, O. Gutowski, P.-A. Carlsson, M. Skoglundh, and E. Lundgren: Science **343** (2014) 758.

[121] E. Chason, T. Mayer, A. Payne, and D. Wu: Applied Physics Letters **60** (1992) 2353.

[122] T. Metzger, C. Luidl, U. Pietsch, and U. Vierl: Nuclear Instruments and Methods in Physics Research Section A: Accelerators, Spectrometers, Detectors and Associated Equipment **350** (1994) 398.

[123] F. Neissendorfer, U. Pietsch, G. Brezesinski, and H. Möwald: Measurement Science and Technology **10** (1999) 354.

[124] J. Malaurent, H. Duval, J. Chauvineau, O. Hainaut, A. Raynal, and P. Dhez: Optics Communications **173** (2000) 255.

[125] S. Roser, R. Felici, and A. Eaglesham: Langmuir **10** (1994) 3853.

[126] B. Paci, A. Generosi, V. Albertini, P. Perfetti, R. De Bettignies, M. Firon, J. Leroy, and C. Sentein: Applied Physics Letters **87** (2005) 194110.

[127] S. Kowarik, A. Gerlach, W. Leitenberger, J. Hu, G. Witte, C. Wöl, U. Pietsch, and F. Schreiber: Thin Solid Films **515** (2007) 5606.

[128] V. Rossi Albertini, B. Paci, and A. Generosi: Journal of Physics D: Applied Physics **39** (2006) R461.

[129] A. Naudon, J. Chihab, P. Goudeau, and J. Mimault: Journal of Applied Crystallography **22** (1989) 460.

[130] U. Niggemeier, K. Lischka, W. M. Plotz, and V. Holy: Journal of Applied Crystallography **30** (1997) 905.

[131] M. Mizusawa and K. Sakurai: IOP Conference Series: Materials Science and Engineering **24** (2011) 012013.

[132] W. Voegeli, C. Kamezawa, E. Arakawa, Y. Yano, T. Shirasawa, T. Takahashi, and T. Matsushita: Journal of Applied Crystallography **50** (2017) 570.

[133] M. Tabuchi, H. Tameoka, T. Kawase, and Y. Takeda: Transactions of the Materials Research Society of Japan **34** (2009) 589.

[134] M. Tabuchi, H. Tameoka, T. Kawase, and Y. Takeda: IOP Conference Series: Materials Science and Engineering **24** (2011) 012007.

[135] H. Tameoka, T. Kawase, M. Tabuchi, and Y. Takeda: Physica Status Solidi (C) Current Topics in Solid State Physics **8** (2011) 294.

[136] P. Kraft, A. Bergamaschi, C. Broennimann, R. Dinapoli, E. Eikenberry, B. Henrich, I. Johnson, A. Mozzanica, C. Schlepüz, P. Willmott, and B. Schmitt: Journal of Synchrotron Radiation **16** (2009) 368.

[137] T. Matsushita, T. Takahashi, T. Shirasawa, E. Arakawa, H. Toyokawa, and H. Tajiri: Journal of Applied Physics **110** (2011) 102209.

[138] W. Voegeli, T. Matsushita, E. Arakawa, T. Shirasawa, T. Takahashi, and Y. Yano: Journal of Physics: Conference Series **425** (2013) 092003.

[139] T. Matsushita, E. Arakawa, W. Voegeli, and Y. Yano: Journal of Synchrotron Radiation **20** (2013) 80.

[140] E. Arakawa, W. Voegeli, T. Matsushita, Y. Yano, and T. Hatano: Journal of Physics: Conference Series **425** (2013) 092002.

[141] Y. Yano, E. Arakawa, W. Voegeli, and T. Matsushita: Journal of Synchrotron Radiation **20** (2013) 980.

[142] T. Uemura, M. Yamagishi, S. Ono, and J. Takeya: Applied Physics Letters **95** (2009) 103301.

[143] H. Yuan, H. Shimotani, A. Tsukazaki, A. Ohtomo, M. Kawasaki, and Y. Iwasa: Advanced Functional Materials **19** (2009) 1046.

[144] Y. Kaji, K. Ogawa, R. Eguchi, H. Goto, Y. Sugawara, T. Kambe, K. Akaike, S. Gohda, A. Fujiwara, and Y. Kubozono: Organic Electronics: physics, materials, applications **12** (2011) 2076.

[145] T. Fujimoto and K. Awaga: Physical Chemistry Chemical Physics **15** (2013) 8983.

[146] K. Ueno, H. Shimotani, H. Yuan, J. Ye, M. Kawasaki, and Y. Iwasa: Journal of the Physical Society of Japan **83** (2014) 032001.

[147] J. Vatamanu and D. Bedrov: Journal of Physical Chemistry Letters **6** (2015) 3594.

[148] A. Kornyshev: Journal of Physical Chemistry B **111** (2007) 5545.

[149] M. Fedorov and A. Kornyshev: Chemical Reviews **114** (2014) 2978.

[150] J. Wang, B. Ocko, A. Davenport, and H. Isaacs: Physical Review B **46** (1992) 10321.

[151] M. Nakamura, N. Sato, N. Hoshi, and O. Sakata: ChemPhysChem **12** (2011) 1430.

[152] M. Nakamura, H. Kaminaga, O. Endo, H. Tajiri, O. Sakata, and N. Hoshi: The Journal of Physical Chemistry C **118** (2014) 22136.

[153] M. Mezger, H. Schröder, H. Reichert, S. Schramm, J. Okasinski, S. Schöder, V. Honkimäki, M. Deutsch, B. Ocko, J. Ralston, M. Rohwerder, M. Stratmann, and H. Dosch: Science **322** (2008) 424.

[154] R. Hayes, N. Borisenko, M. Tam, P. Howlett, F. Endres, and R. Atkin: Journal of Physical Chemistry C **115** (2011) 6855.

[155] R. Yamamoto, H. Morisaki, O. Sakata, H. Shimotani, H. Yuan, Y. Iwasa, T. Kimura, and Y. Wakabayashi: Applied Physics Letters **101** (2012) 053122.

[156] W. Voegeli, E. Arakawa, T. Matsushita, O. Sakata, and Y. Wakabayashi: Zeitschrift für Physikalische Chemie **230** (2016) 577.

[157] A. Uysal, H. Zhou, G. Feng, S. Lee, S. Li, P. Fenter, P. Cummings, P. Fulvio, S. Dai, J. McDonough, and Y. Gogotsi: Journal of Physical Chemistry C **118** (2014) 569.

[158] T. Petach, A. Mehta, R. Marks, B. Johnson, M. Toney, and D. Goldhaber-Gordon: ACS Nano **10** (2016) 4565.

[159] H. Yuan, H. Shimotani, J. Ye, S. Yoon, H. Aliah, A. Tsukazaki, M. Kawasaki, and Y. Iwasa: Journal of the American Chemical Society **132** (2010) 18402.

[160] S. Makino, Y. Kitazumi, N. Nishi, and T. Kakiuchi: Electrochemistry Communications **13** (2011) 1365 .

[161] B. Roling, M. Druschler, and B. Huber: Faraday Discuss. **154** (2012) 303.

[162] N. Nishi, Y. Hirano, T. Motokawa, and T. Kakiuchi: Phys. Chem. Chem. Phys. **15** (2013) 11615.

[163] M. Sha, G. Wu, Q. Dou, Z. Tang, and H. Fang: Langmuir **26** (2010) 12667.

[164] J. Vatamanu, L. Xing, W. Li, and D. Bedrov: Phys. Chem. Chem. Phys. **16** (2014) 5174.

[165] C. Péan, C. Merlet, B. Rotenberg, P. A. Madden, P.-L. Taberna, B. Daffos, M. Salanne, and P. Simon: ACS Nano **8** (2014) 1576.

[166] R. Wang, K. Hashimoto, A. Fujishima, M. Chikuni, E. Kojima, A. Kitamura, M. Shimohigoshi, and T. Watanabe: Nature **388** (1997) 431.

[167] R. Wang, K. Hashimoto, A. Fujishima, M. Chikuni, E. Kojima, A. Kitamura, M. Shimohigoshi, and T. Watanabe: Advanced Materials **10** (1998) 135.

[168] H. Irie, K. Sunada, and K. Hashimoto: Electrochemistry **72** (2004) 807.

[169] K. Hashimoto, H. Irie, and A. Fujishima: Japanese Journal of Applied Physics **44** (2005) 8269.

[170] J. M. White, J. Szanyi, and M. A. Henderson: The Journal of Physical Chemistry B **107** (2003) 9029.

[171] J. Yates Jr.: Surface Science **603** (2009) 1605.

[172] T. Zubkov, D. Stahl, T. L. Thompson, D. Panayotov, O. Diwald, and J. T. Yates: The Journal of Physical Chemistry B **109** (2005) 15454.

[173] T. L. Thompson and J. T. Yates: Chemical Reviews **106** (2006) 4428.

[174] N. Ohtsu, N. Masahashi, Y. Mizukoshi, and K. Wagatsuma: Langmuir **25** (2009) 11586.

[175] N. Ishida and D. Fujita: Journal of Vacuum Science & Technology A: Vacuum, Surfaces, and Films **30** (2012) 051402.

[176] R. Wang, N. Sakai, A. Fujishima, T. Watanabe, and K. Hashimoto: The Journal of Physical Chemistry B **103** (1999) 2188.

[177] M. Miyauchi, A. Nakajima, A. Fujishima, K. Hashimoto, and T. Watanabe: Chemistry of Materials **12** (2000) 3.

[178] N. Sakai, A. Fujishima, T. Watanabe, and K. Hashimoto: The Journal of Physical Chemistry B **105** (2001) 3023.

[179] A. Nakajima, S. Koizumi, T. Watanabe, and K. Hashimoto: Journal of Photochemistry and Photobiology A: Chemistry **146** (2001) 129.

[180] R.-D. Sun, A. Nakajima, A. Fujishima, T. Watanabe, and K. Hashimoto: The Journal of Physical Chemistry B **105** (2001) 1984.

[181] N. Sakai, A. Fujishima, T. Watanabe, and K. Hashimoto: The Journal of Physical Chemistry B **107** (2003) 1028.

[182] H. Irie and K. Hashimoto: *Environmental Photochemistry Part II*, ed. P. Boule, D. W. Bahnemann, and P. K. J. Robertson (Springer Berlin Heidelberg, Berlin, Heidelberg, 2005) pp. 425–450.

[183] L.-M. Liu, C. Zhang, G. Thornton, and A. Michaelides: Phys. Rev. B **82** (2010) 161415.

[184] L. Yang, D.-J. Shu, S.-C. Li, and M. Wang: Phys. Chem. Chem. Phys. **18** (2016) 14833.

[185] T. Shirasawa, W. Voegeli, E. Arakawa, T. Takahashi, and T. Matsushita: The Journal of Physical Chemistry C **120** (2016) 29107.

[186] Z. Zhang, P. Fenter, N. C. Sturchio, M. J. Bedzyk, M. L. Machesky, and D. J. Wesolowski: Surface Science **601** (2007) 1129 .

[187] T. Ohto, A. Mishra, S. Yoshimune, H. Nakamura, M. Bonn, and Y. Nagata: Journal of Physics: Condensed Matter **26** (2014) 244102.

[188] S. Tan, H. Feng, Y. Ji, Y. Wang, J. Zhao, A. Zhao, B. Wang, Y. Luo, J. Yang, and J. G. Hou: Journal of the American Chemical Society **134** (2012) 9978.

[189] A. V. Bandura, D. G. Sykes, V. Shapovalov, T. N. Troung, J. D. Kubicki, and R. A. Evarestov: The Journal of Physical Chemistry B **108** (2004) 7844.

[190] T. Seydel, A. Madsen, M. Tolan, G. Grübel, and W. Press: Phys. Rev. B **63** (2001) 073409.

[191] M. S. Pierce, K. C. Chang, D. Hennessy, V. Komanicky, M. Sprung, A. Sandy, and H. You: Phys. Rev. Lett. **103** (2009) 165501.